

## Porphyrin Distortion during Affinity Maturation of a Ferrochelatase Antibody, Monitored by Resonance Raman Spectroscopy

Swarnalatha Venkatesh Rao,<sup>†</sup> Jun Yin,<sup>‡,§,||</sup> Andrzej A. Jarzęcki,<sup>†,⊥</sup>  
Peter G. Schultz,<sup>§,∇</sup> and Thomas G. Spiro<sup>\*,†</sup>

Contribution from the Department of Chemistry, Princeton University, Princeton, New Jersey 08544, Department of Chemistry, University of California, Berkeley, California 94720, and Department of Chemistry and The Skaggs Institute of Chemical Biology, The Scripps Research Institute, La Jolla, California 92037

Received June 11, 2004; E-mail: spiro@princeton.edu

**Abstract:** Resonance Raman (RR) spectra are reported for mesoporphyrin IX bound to the Fab fragment of the ferrochelatase antibody 7G12. Binding induces activation of a Raman band at 680 cm<sup>-1</sup>, which is assigned to an out-of-plane porphyrin vibration,  $\gamma_{15}$ . This is exactly the predicted effect of distorting mesoporphyrin to the geometry of *N*-methylmesoporphyrin IX, the 7G12 hapten, based on DFT/CIS modeling of the RR spectrum. The modeling also shows that the pyrrole ring that is tilted out of the porphyrin plane bears a nitrogen lone pair, which is therefore available for coordination by an incoming metal ion. The 680 cm<sup>-1</sup> band intensity is ~3 times higher for the affinity-matured antibody than for the germline precursor antibody, while intermediate values are found for variants in which germline residues are mutated to mature residues or vice versa. Thus, RR spectroscopy reveals an evolution from weak substrate distortion in the germline antibody to strong substrate distortion in the affinity-matured antibody, and supports the view that catalysis involves a substrate strain mechanism.

### Introduction

The enzyme ferrochelatase has inspired the development of a catalytic antibody,<sup>1</sup> whose maturation via somatic mutations has been analyzed structurally.<sup>2</sup> This system exemplifies in atomic detail the roles of induced fit<sup>3</sup> and of strain<sup>4</sup> in enzymatic catalysis.

Ferrochelatase catalyzes the insertion of Fe<sup>2+</sup> into protoporphyrin IX as the last step in heme biosynthesis.<sup>5</sup> In vitro, the enzyme can accept other porphyrins, such as mesoporphyrin IX (MP; Figure 1), and other divalent ions, such as Zn<sup>2+</sup> and Co<sup>2+</sup>. Ferrochelatase is strongly inhibited by *N*-alkylated porphyrins, suggesting that porphyrin distortion, which is induced by *N*-alkylation, serves to increase the insertion rate, by exposing the pyrrole nitrogen lone pairs to the metal.<sup>6–8</sup>

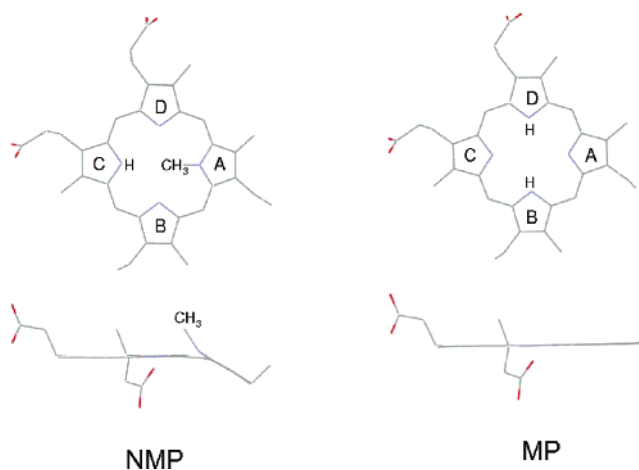


**Figure 1.** Structural diagrams of NMP and MP molecules. The side view illustrates the 32° tilt of the NMP A ring, and a slight porphyrin saddling.

Theoretical modeling of the ferrochelatase active site via QM/MM computation suggests significant porphyrin distortion by the enzyme.<sup>9</sup>

Antibodies raised to *N*-methylmesoporphyrin IX (NMP; Figure 1) have been found to catalyze divalent metal ion insertion into MP with rates comparable to that of ferroche-

<sup>†</sup> Princeton University.

<sup>‡</sup> University of California.

<sup>§</sup> Department of Chemistry, The Scripps Research Institute.

<sup>||</sup> Current address: Department of Biological Chemistry and Molecular Pharmacology, Harvard Medical School, 240 Longwood Ave., Boston, MA 02115.

<sup>⊥</sup> Current address: Department of Chemistry, Brooklyn College, The City University of New York, Brooklyn, NY 11210.

<sup>∇</sup> The Skaggs Institute of Chemical Biology, The Scripps Research Institute.

(1) Cochran, A. G.; Schultz, P. G. *Science* **1990**, *249*, 781–783.  
(2) Yin, J.; Andryski, S. E.; Beuscher, A. E.; Stevens, R. C.; Schultz, P. G. *Proc. Natl. Acad. Sci. U.S.A.* **2003**, *100*, 856–861.  
(3) Koshland, D. E. *Proc. Natl. Acad. Sci. U.S.A.* **1958**, *44*, 98–104.  
(4) Haldane, J. B. S. *Enzymes*; Longmans Green: London, 1930.  
(5) Dailey, H. A.; Dailey, T. A.; Wu, C. K.; Medlock, A. E.; Wang, K. F.; Rose, J. P.; Wang, B. C. *Cell. Mol. Life Sci.* **2000**, *57*, 1909–1926.  
(6) McLaughl, Gm. *J. Chem. Soc., Perkin Trans. 2* **1974**, 136–140.

(7) Dailey, H. A. In *Mechanisms of Metallocenter Assembly*; Marzilli, C. G., Ed.; VCH: New York, 1996; pp 77–89.  
(8) Lavalley, D. K. In *Mechanistic Principles of Enzyme Activity*; Greeberg, A., Ed.; VCH: New York, 1988; pp 279–314.  
(9) Sigfridsson, E.; Ryde, U. *J. Biol. Inorg. Chem.* **2003**, *8*, 273–282.

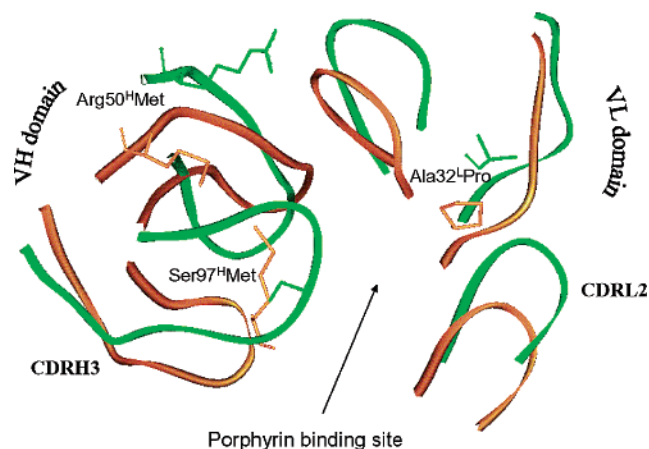


**Figure 2.** Porphyrin binding region of ligand-free germline (PDB code 1NGZ, green) and affinity-matured (PDB code 1NGY, brown) 7G12 antibody. The three (out of five) somatic mutations, closest to the binding site are shown. Two more distant somatic mutations are Ser76<sup>H</sup>Asn and Ser14<sup>L</sup>Thr. H and L denote heavy and light chains.

lase.<sup>1</sup> X-ray crystallography has established significant distortion of MP when bound to the Fab fragment of antibody 7G12, evidence that the substrate is strained by the enzyme toward its transition state.<sup>2</sup>

The 7G12 germline precursor shows marked structural differences relative to the affinity-matured antibody (Figure 2). The porphyrin binding cleft is flanked by loops from the V<sub>H</sub> and V<sub>L</sub> domains, which have significantly different dispositions in the germline and mature proteins.<sup>2</sup> When hapten binds to the germline antibody, these loops are displaced toward the positions seen in the affinity-matured antibody, whereas little motion occurs in the latter when hapten is bound. Thus, the germline binding site is a good example of induced fit. The energetic cost of the protein rearrangement is reflected in the 100-fold lower binding affinity for the germline relative to the affinity-matured antibody.<sup>2</sup> There are five somatic mutations between germline and mature antibody. Proteins with individual mutations have hapten affinities that are intermediate between those of germline and mature antibody,<sup>2</sup> and provide an opportunity to trace the evolution of strong binding.

Resonance Raman spectra are sensitive to porphyrin structure, and can be used to monitor out-of-plane distortions.<sup>10,11</sup> Out-of-plane vibrational modes are not resonance-enhanced for planar porphyrins, but are activated by out-of-plane distortions. In previous work we have detected such activation for MP bound to ferrochelatase on one hand<sup>12</sup> and the 7G12 antibody on the other.<sup>13</sup> Different modes were detected in the two cases, suggesting that while the substrate is distorted by both enzymes, the distorted geometry is different.

In this work, we model the RR activation induced by antibody 7G12, using computational methods which are described elsewhere.<sup>10</sup> The activation is predicted by the NMP hapten geometry. In addition, the modeling indicates that the tilted pyrrole ring bears a lone pair on the N atom, as required for antibody-catalyzed metal insertion.

- (10) Jarzecki, A. A.; Spiro, T. G. *J. Phys. Chem. A* **2005**, in press.  
 (11) Shelnutz, J. A.; Song, X. Z.; Ma, J. G.; Jia, S. L.; Jentzen, W.; Medforth, C. J. *Chem. Soc. Rev.* **1998**, *27*, 31–41.  
 (12) Blackwood, M. E.; Rush, T. S.; Romesberg, F.; Schultz, P. G.; Spiro, T. G. *Biochemistry* **1998**, *37*, 779–782.  
 (13) Blackwood, M. E.; Rush, T. S.; Medlock, A.; Dailey, H. A.; Spiro, T. G. *J. Am. Chem. Soc.* **1997**, *119*, 12170–12174.

The extent of activation is much less for germline than for affinity-matured antibody, while variants with individual somatic mutations show intermediate activation. Thus, the induced fit binding of the germline antibody produces less porphyrin distortion. Not only is the affinity-matured antibody preorganized for substrate binding, but the binding produces greater strain in the substrate.

## Methods

**Preparation of Samples.** The preparation and purification of Fab fragments of affinity-matured antibody 7G12 and of its germline precursor, as well as variants with individual residue replacements, have been described elsewhere.<sup>2,14,15</sup> Mesoporphyrin IX free base (MP) and its *N*-methylated product (NMP) were obtained from Midcentury Chemicals (Posen, IL). A stock solution was prepared by first dissolving the porphyrin in 50  $\mu$ L of NH<sub>4</sub>OH, and adding 250  $\mu$ L of 5% (w/v) Triton-X 100 and 700  $\mu$ L of water. Further dilutions were made by using 50 mM Tris–HCl buffer, at pH 8.0. Samples containing 50  $\mu$ M MP and 70  $\mu$ M protein in Tris buffer, pH 8.0 (antibody being kept in slight excess to avoid unbound porphyrin) were purged with N<sub>2</sub> for 20 min and then used for Raman measurements. The proteins were (a) germline 7G12 Fab, (b) affinity-matured 7G12 Fab, (c) three “up” mutants (single mutations of the germline antibody among the known somatic mutations), Ala32<sup>L</sup>Pro, Arg50<sup>H</sup>Met, and Ser97<sup>H</sup>Met, (d) three “down” mutants (single reverse mutations from the affinity-matured antibody), Pro32<sup>L</sup>Ala, Met50<sup>H</sup>Arg, and Met97<sup>H</sup>Ser, and (e) “chain-swap” mutants (heavy and light chains of the germline and affinity-matured antibodies are swapped: V<sub>L</sub> germline, germline light chain and affinity-matured heavy chain; V<sub>H</sub> germline, germline heavy chain and affinity-matured light chain).

We found that the 680 cm<sup>-1</sup> shoulder, assigned to  $\gamma_{15}$  (see the Results) increased with time when the solutions were allowed to sit in the cold room under N<sub>2</sub> and protected from light; this effect leveled off after 4 days. Apparently some steps in substrate binding are slow. All reported spectra and concentrations were for solutions that had been stored for 4 days.

**Spectroscopy.** Resonance Raman spectra were obtained in spinning NMR tubes using the 406.7 nm excitation line from a Spectra-Physics Beamlok 2080 krypton ion laser with 135° backscattering geometry. Laser power at the sample ranged between 8 and 15 mW. The scattered light was collected and focused onto the slit of a Spex 1877 triple monochromator equipped with a 2400 grooves/mm grating and detected using a diode array detector. Spectral acquisition times were typically 15 min.

**Computation.** RR spectra were modeled via electronic structure calculations on MP, as described elsewhere.<sup>10</sup> Geometries and vibrational mode compositions and frequencies were computed using density functional theory with nonlocal, Becke three-parameter exchange and Lee–Young–Parr correlation functionals (B3LYP) and 6-31G\* basis functions, as implemented in the Gaussian 98 suite of programs.<sup>16</sup> To improve on the quality of the normal modes, the scaled quantum mechanical (SQM) refinement of DFT force constants by transferable

- (14) Romesberg, F. E.; Santarsiero, B. D.; Spiller, B.; Yin, J.; Barnes, D.; Schultz, P. G.; Stevens, R. C. *Biochemistry* **1998**, *37*, 14404–14409.  
 (15) Ulrich, H. D.; Patten, P. A.; Yang, P. L.; Romesberg, F. E.; Schultz, P. G. *Proc. Natl. Acad. Sci. U.S.A.* **1995**, *92*, 11907–11911.  
 (16) Frisch, M. J.; Trucks, G. W.; Schlegel, H. B.; Scuseria, G. E.; Robb, M. A.; Cheeseman, J. R.; Zakrzewski, V. G.; Montgomery, J. A., Jr.; Stratmann, R. E.; Burant, J. C.; Dapprich, S.; Millam, J. M.; Daniels, A. D.; Kudin, K. N.; Strain, M. C.; Farkas, O.; Tomasi, J.; Barone, V.; Cossi, M.; Cammi, R.; Mennucci, B.; Pomelli, C.; Adamo, C.; Clifford, S.; Ochterski, J.; Petersson, G. A.; Ayala, P. Y.; Cui, Q.; Morokuma, K.; Malick, D. K.; Rabuck, A. D.; Raghavachari, K.; Foresman, J. B.; Cioslowski, J.; Ortiz, J. V.; Baboul, A. G.; Stefanov, B. B.; Liu, G.; Liashenko, A.; Piskorz, P.; Komaromi, I.; Gomperts, R.; Martin, R. L.; Fox, D. J.; Keith, T.; Al-Laham, M. A.; Peng, C. Y.; Nanayakkara, A.; Gonzalez, C.; Challacombe, M.; Gill, P. M. W.; Johnson, B. G.; Chen, W.; Wong, M. W.; Andres, J. L.; Head-Gordon, M.; Replogle, E. S.; Pople, J. A. *Gaussian 98*, Revision A.7; Gaussian, Inc.: Pittsburgh, PA, 1998.

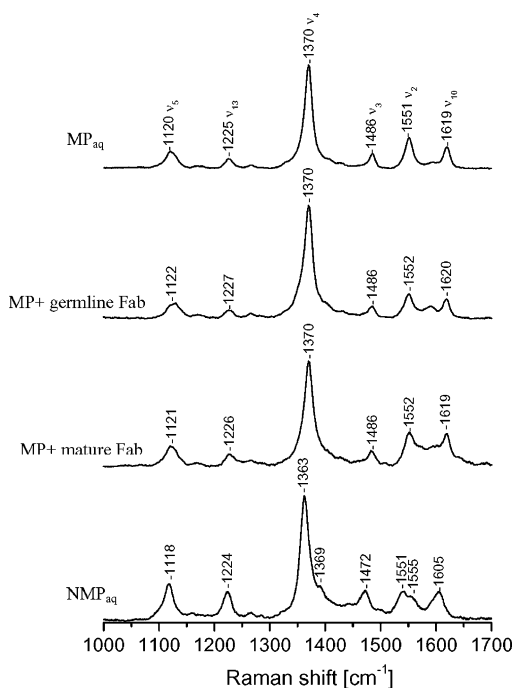


**Figure 3.** Porphyrin bond stretching region of the 406.7 nm excited RR spectra of MP and NMP in aqueous solution (top and bottom) and of MP bound to Fab fragments of germline or affinity-matured 7G12 antibody.

scale factors was employed.<sup>17,18</sup> The resonance Raman intensity patterns enhanced via excitation near the Soret electronic transitions were computed from vertical gradients on the resonant states, evaluated at the CIS (configuration interaction with single excitations) level of theory.<sup>10</sup>

## Results

**Spectroscopy.** Figure 3 displays RR spectra of MP in aqueous solution and bound to antibody, in the region of porphyrin bond stretching vibrations (for mode labeling, see ref 10). The spectra are almost identical. The effect of antibody binding is limited to a broad weak feature between the 1619 ( $\nu_{10}$ ) and 1551 ( $\nu_2$ )  $\text{cm}^{-1}$  bands, probably reflecting a modest activation of infrared modes in this region. Similar activation is seen for aqueous NMP (bottom spectrum in Figure 3). We note that more substantial perturbations of the MP spectrum were reported in our earlier antibody binding study.<sup>13</sup> It seems likely that the earlier solutions contained impurities; there may have been some degradation of MP, which is sensitive to light and oxygen. Although the intensity pattern is similar, the mode frequencies are systematically lower for NMP than MP. This is an electronic effect of the methylation, and is captured by DFT computations, as discussed elsewhere.<sup>10</sup>

In the low-frequency region (Figure 4), the spectra are also very similar, but antibody binding induces a 676  $\text{cm}^{-1}$  shoulder on the 661  $\text{cm}^{-1}$   $\nu_7$  band. This shoulder is quite distinct for MP bound to affinity-matured antibody, and also for aqueous NMP, where it is shifted slightly, to 680  $\text{cm}^{-1}$ . The shoulder is assigned to an out-of-plane mode, designated  $\gamma_{15}$ , by analogy with a saddling-type mode (see the eigenvector in Figure 5

of the computational paper<sup>10</sup>) of NiOEP or the artificial model porphyrin FBP-X<sub>8</sub>.<sup>10</sup> There is also an asymmetric broadening

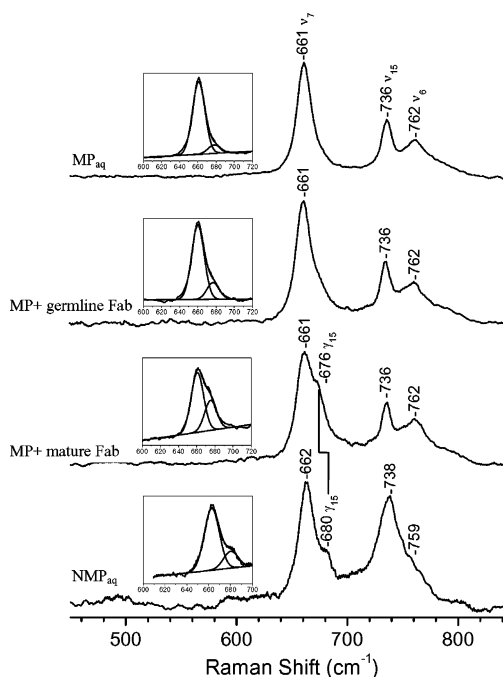


**Figure 4.** Low-frequency region of the 406.7 nm excited RR spectra of MP and NMP in aqueous solution (top and bottom) and of MP bound to Fab fragments of germline or affinity-matured 7G12 antibody. The out-of-plane  $\gamma_{15}$  mode is activated in NMP, and upon 7G12 antibody binding to MP. Deconvolution of the  $\gamma_{15}$  band is shown in the insets.

of the 762  $\text{cm}^{-1}$  band, which we attribute to augmentation of another out-of-plane mode,  $\gamma_{6, \text{NH}}$  (see below). The activation of  $\gamma_{15}$  was reported in our earlier study,<sup>13</sup> but again we note the presence of additional bands in the earlier spectrum, which probably arose from impurities. The present results indicate that the only substantial effect of antibody binding is activation of  $\gamma_{15}$ .

Five somatic mutations accumulate during the affinity maturation process of the 7G12 germline antibody: two in the V<sub>L</sub> chain (Ser14<sup>L</sup>Thr and Ala32<sup>L</sup>Pro) and three in V<sub>H</sub> (Arg50<sup>H</sup>Met, Ser76<sup>H</sup>Asn, and Ser97<sup>H</sup>Met). The effects of these mutations on mesoporphyrin can be quantitated by spectral analysis of mutants of the germline and affinity-matured antibody in which somatic mutations are individually introduced (up mutants) or deleted (down mutants). The  $\gamma_{15}$  intensity relative to that of the adjacent  $\nu_7$ , via band deconvolution (Figure 4 insets), is nearly 3 times higher for the affinity-matured than for the germline antibody. Intensities for mutant antibodies are intermediate (Figure 5). As might be expected, the up mutants (entries 1–3 in Figure 5), which contain one of the five somatic mutations introduced into the germline antibody, have weaker  $\gamma_{15}$  activation than the down mutants (entries 5–7 in Figure 5), in which one of these five mutations is deleted from the affinity-matured antibody. Interestingly, the two chain-swap variants show different extents of activation; the  $\gamma_{15}$  intensity is higher when the light chain is from the germline than when it is from the affinity-matured antibody. The heavy chain appears to dominate the activation.

**Computation.** As described in our computational paper,<sup>10</sup> porphyrin RR spectra can be computed via a combination of DFT-SQM determination of the ground-state force field and CIS evaluation of resonant excited-state gradients for the ground-state normal modes. Predicted and experimental spectra were

(17) Rauhut, G.; Pulay, P. *J. Am. Chem. Soc.* **1995**, *117*, 4167.

(18) Baker, J.; Jarzecki, A. A.; Pulay, P. *J. Phys. Chem. A* **1998**, *102*, 1412–1424.

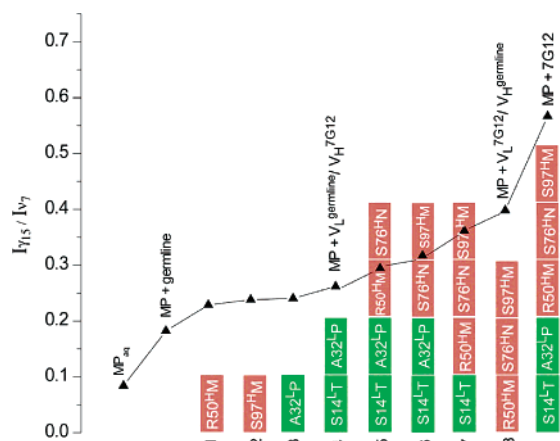


**Figure 5.** Intensity of the  $680\text{ cm}^{-1}$   $\gamma_{15}$  band, relative to the  $662\text{ cm}^{-1}$   $\nu_7$  band, for MP bound to the germline Fab, the affinity-matured Fab, and various mutants of the germline Fab numbered 1–8. The identities of the somatic mutations in the mutants are labeled on the bars. Green bars denote the light-chain somatic mutations, while red bars denote the heavy-chain somatic mutations.

found to match quite well for free base porphine and MP, and also for the distorted porphyrin NMP, which is the hapten for the 7G12 antibody.

When applied to unconstrained MP, the DFT-SQM/CIS methodology models the observed RR spectrum of aqueous MP satisfactorily.<sup>10</sup> The low-frequency spectra are compared in Figure 6 (the two black traces), where it can be seen that the frequencies and relative intensities of the principal observed features, the bands assigned to the in-plane porphyrin modes  $\nu_7$ ,  $\nu_{15}$ , and  $\nu_6$ , are predicted with the correct frequencies and intensity pattern. The main shortcoming of the computation is overestimation of the intensities of the infrared-active modes  $\nu_{45}$ ,  $\nu_{46}$ , and  $\nu_{48}$ .<sup>10</sup> Their RR activation is due to the loss of the porphyrin center of symmetry, which is associated with the asymmetric distribution of the peripheral substituents in MP (Figure 1). This effect is overemphasized in the CIS gradients. We note that there is some activation of out-of-plane (oop) modes (see Table 4 of ref 10), even though the unconstrained porphyrin is flat. This effect is due to the ethyl and propionate substituents (Figure 1) being oriented out of the plane, and contributing to the eigenvectors of the oop skeletal modes. The biggest effect is seen for the  $\gamma_{6,\text{NH}}$  mode, which is nearly as strong as the adjacent  $\nu_6$  band, and contributes to the broad band envelope, a feature of the experimental as well as the computed spectra.

We then computed spectra for MP in various constrained geometries, a procedure that has been evaluated using the artificial porphyrin FBP- $X_8$ .<sup>10</sup> When MP was constrained to the coordinates reported in the crystal structure of MP-bound mature Fab, the predicted spectrum (Figure 6, top) bore no resemblance to the observed spectrum. The predicted spectrum is dominated by features whose computed eigenvectors mainly involve motions of the MP substituents; the porphyrin skeletal modes are weak in comparison. We infer that the CIS gradients become unreliable for the type and extent of distortion in the reported structure.

On the other hand, the structure of the NMP hapten serves very well (red trace) to model the observed spectrum. As seen in Figure 6 (spectrum marked  $\text{MP}_{\text{NMP(BD)}}$ ) the effect of distorting MP to the NMP porphyrin geometry is to induce activity in

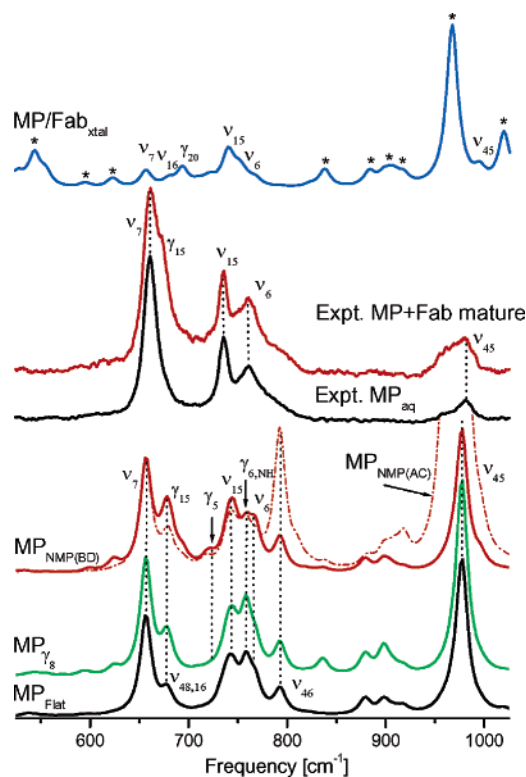


**Figure 6.** Experimental (MP and 7G12-bound MP) and modeled RR spectra. In the modeling, the MP was unconstrained ( $\text{MP}_{\text{Flat}}$ , bottom) or constrained to the protein crystal coordinates ( $\text{MP}/\text{Fab}_{\text{xtal}}$ , top), along the  $\gamma_8$  distortion coordinate ( $\text{MP}_{\gamma_8}$ , green), or to the NMP porphyrin geometry ( $\text{MP}_{\text{NMP}}$ , red). In the last case, the protons were on pyrrole rings B and D, lying near the mean porphyrin plane (solid line) or on rings A and C, one of which (A) is tilted out of the plane (dotted line). Asterisks on the  $\text{MP}/\text{Fab}_{\text{xtal}}$  spectrum indicate modes whose eigenvectors contain dominant contributions from the MP peripheral substituents.

$\nu_{15}$ , on the side of the  $\nu_7$  band. This is exactly the effect observed when MP is bound to mature Fab. There is also some broadening of the complex band arising from the overlap of  $\nu_6$  with  $\gamma_{6,\text{NH}}$ , and this is also detectable in the experimental spectrum. The intensities of the infrared modes continue to be overestimated, as they are in the unconstrained MP calculation. Contributions of the various vibrational modes to the computed intensities are given in Table 4 of ref 10.

Clearly, the RR spectrum favors the NMP structure over the protein crystal structure. The two structures are compared in Figure 7. In NMP pyrrole ring A is tilted  $32^\circ$  out of the mean plane, and there is a saddling displacement of the porphyrin as a whole. This saddling is seen in the protein structure as well, but there is also substantial ruffling, and the D and A rings are both tilted out of the plane. The maximum deviation of any single atom between the two structures is  $0.8\text{ \AA}$  ( $C_m$  atom between rings C and D), while the mean square displacement of the porphyrin skeleton from the average plane is slightly greater for NMP,  $0.065\text{ \AA}$ , than for the protein structure,  $0.053\text{ \AA}$ . In view of the limited resolution,  $2.60\text{ \AA}$ , of the protein crystal structure, it is doubtful that these differences are experimentally significant. (We note that crystallography at  $2.40\text{ \AA}$  resolution has shown that NMP binds to mature 7G12 antibody with the same geometry as in NMP crystals<sup>14</sup>). Nevertheless, the predicted RR spectrum is highly sensitive to the structural differences.

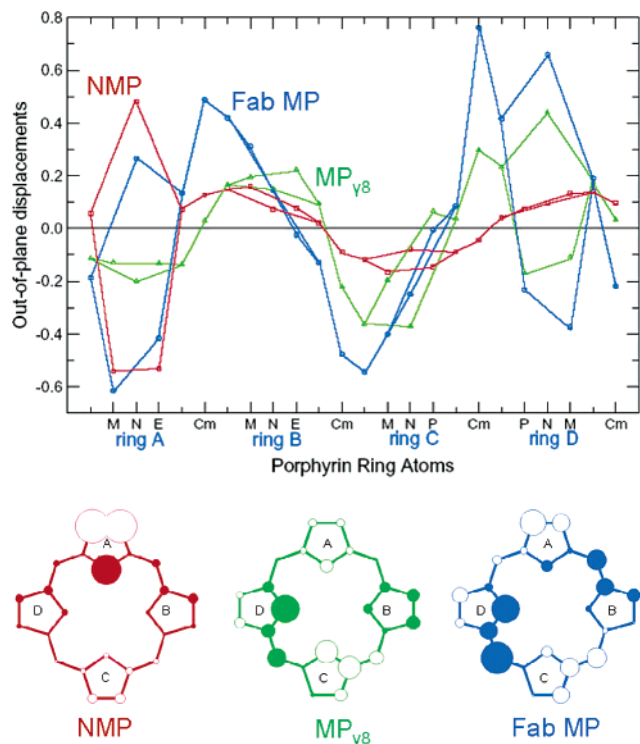


**Figure 7.** (Top) Connectivity plot of out-of-plane displacements for NMP (red), MP in the Fab–MP crystal structure (blue), and MP distorted along  $\gamma_8$  to the same average out-of-plane displacement (0.053 Å) as in Fab–MP. (Bottom) Projection of the atomic out-of-plane displacements in the three structures. The size of the circles is proportional to the extent of displacement.

To see whether the agreement with experiment is unique to the NMP structure, we systematically computed RR spectra by distorting the NMP along each of the 17 normal modes of MP, which are computed to lie below  $200\text{ cm}^{-1}$ . None of these produced a pattern close to experiment, except for distortion along the mode assigned to  $\gamma_8$ . This is a kind of saddling distortion (see Figure 5 of the computational paper<sup>10</sup> for the parent eigenvector), although in the low-symmetry framework of MP, there are additional localized displacements, including tilting of the D ring. Figure 7 shows the resulting structure, constrained to the same mean square displacement from the average porphyrin plane,  $0.053\text{ Å}$ , as seen in the protein crystal structure. The computed spectrum, shown in Figure 6 (green trace), resembles that of the NMP-constrained structure, but the  $\gamma_{6,\text{NH}}$  mode is slightly exaggerated, while the  $\gamma_{15}$  enhancement is too low. Thus, the NMP structure reproduces the experimental spectrum, especially the  $\gamma_{15}$  activation, significantly better than does distortion along  $\gamma_8$ .

It is likely that agreement with the experimental RR spectrum could be improved with some linear combination of the various possible distortion coordinates. We have not attempted to explore this large conformational space, since there is no objective criterion for evaluating the results, given the imperfect character of the spectral computation.

The conclusion we draw from this analysis is that constraining MP to the NMP structure produces a computed RR spectrum which is remarkably close to the experimental MP–Fab spectrum. Moreover, the RR spectrum is clearly very sensitive to the form of the distortion. While the NMP fit may not be

unique, there is no obvious alternative structure which does as well.

Finally, we considered the consequences of NH tautomerization at different pyrrole rings in MP. For the spectrum discussed above,  $\text{MP}_{\text{NMP(BD)}}$ , the protons were placed on the B and D rings, and the N–H bonds are both close to the porphyrin plane. When the protons were placed instead on the A and C rings,  $\text{MP}_{\text{NMP(AC)}}$ , agreement with experiment deteriorated (Figure 7, dashed red trace). Very large enhancements are predicted for the infrared modes  $\nu_{45}$  and  $\nu_{48}$ , whereas the  $\gamma_{15}$  intensity diminishes. These alterations stem from the fact that, in  $\text{MP}_{\text{NMP(AC)}}$ , the proton on the tilted A ring projects out of the porphyrin plane. Clearly, the in-plane tautomer accounts much better for the experimental spectrum.

## Discussion

**Substrate Distortion Matches the Hapten.** The present results provide striking support for the rationale behind the development of catalytic antibodies, namely, that using a transition-state model as the hapten will elicit antibodies that bind and distort the substrate toward the transition state. NMP, a powerful ferrochelatase inhibitor, is believed to model the transition state for metal insertion, and antibodies elicited by NMP do indeed catalyze this reaction.<sup>1</sup> The present RR spectral modeling clearly shows that MP bound to 7G12 antibody does distort toward the NMP porphyrin geometry. The indicator for this distortion is activation of the out-of-plane mode which correlates with  $\gamma_{15}$  of symmetric porphyrins. This activation is the only significant spectral change associated with antibody binding, and is accurately reproduced by the DFT/CIS methodology for RR modeling, when MP is constrained to the NMP structure.

The computed spectra are very sensitive to the nature of the modeled distortion. When MP was distorted along each of the 17 lowest frequency out-of-plane modes, only one, analogous to  $\gamma_8$ , produced a spectrum anything like the experimental spectrum, and it failed to predict significant  $\gamma_{15}$  activation. While some linear combination of these distortion coordinates might have produced a better result, it is likely that the resulting structure would resemble NMP. Although we cannot prove the uniqueness of the NMP result, the sensitivity of the modeled spectra suggests that a good fit is unlikely for any structure deviating substantially from NMP.

This presumption is reinforced by the bad fit obtained for the reported crystallographic structure of bound MP. The spectrum computed for this structure is completely different from the experimental spectrum. Comparison of the structures (Figure 7) suggests that the atomic displacements relative to NMP are not experimentally significant, given the limited resolution ( $2.60\text{ Å}$ ) of the protein crystal structure, but the computed RR spectra are clearly sensitive to these differences.

**Tilted Pyrrole N Bears a Lone Pair.** The computed RR spectra also permit a choice among porphyrin tautomers, information that is otherwise unavailable, since protons cannot be resolved in the protein crystal structure. Agreement with the experimental spectrum is obtained if the protons are located on the pyrrole N atoms which remain in the porphyrin plane. If instead the tilted pyrrole bears a proton, then the computed spectrum differs markedly from the experimental spectrum. Activation of  $\gamma_{15}$  diminishes, while dramatic enhancement is

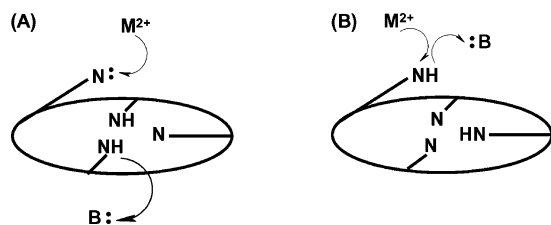


**Figure 8.** Alternative mechanisms for metal ion insertion. (A)  $M^{2+}$  attacks the N lone pair, exposed by pyrrole tilting, followed by proton transfer to the endogenous base. (B) Proton transfer to the endogenous base, followed by metal ion attack. RR spectral modeling, which shows the tilted pyrrole does not bear a proton, favors (A).

predicted for the infrared modes  $\nu_{45}$  and  $\nu_{46}$ . The  $\nu_{45}$  mode is activated only modestly in the experimental spectrum, while  $\nu_{46}$  is activated only weakly, if at all. Thus, the RR spectrum shows that the tilted pyrrole ring does not bear a proton.

This result is important for the mechanism of metal insertion. It is generally assumed that porphyrin distortion exposes a nitrogen lone pair to an incoming metal ion; coordination of the metal ion would then be followed by dissociation of two pyrrole protons, perhaps assisted by a basic residue on the protein. In the 7G12 antibody crystal structures, the assisting base is likely the carboxylate side chain Asp 96, which is close to the pyrrole N atoms.<sup>2</sup>

This view of the mechanism is supported by the present results, which indicate that the pyrrole ring does not bear a proton. If it did, the proton would have to be removed before the incoming metal could access the lone pair. The two alternatives are diagrammed in Figure 8. Since metal ion attack on an exposed lone pair would be diffusion limited, whereas proton transfer would be limited by the  $pK_a$  difference between the porphyrin and the assisting base, alternative A would be more efficient. This is the alternative that is consistent with the RR spectra.

**Evolution of Substrate Strain in Antibody 7G12.** The present RR analysis of the conformation of MP bound to germline Fab, 7G12 Fab, and various mutants provides further insight into the coevolution of the binding and catalytic activity of this antibody. Previously, a comparison of the crystal structures of the ligand-free or NMP-bound germline Fab and the corresponding affinity-matured 7G12 Fab's showed that significant structural rearrangements in the antibody combining site occurred upon binding of the germline antibody with either NMP or a structurally nonrelated small molecule, Jeffamine.<sup>19</sup> However, affinity-matured 7G12 Fab showed minimal changes upon NMP binding and no affinity for Jeffamine. These results suggested an "induced-fit" binding mode for the germline antibody which is characterized by moderate binding affinities with the target antigen and broad binding specificities. In contrast, the affinity-matured antibodies adopt a "lock-and-key" binding mode which is characterized by high-affinity binding with the hapten and stringent binding specificity. This notion is also supported by structural studies on the germline and affinity-matured antibodies 48G7,<sup>20</sup> AZ28,<sup>21</sup> and 28B4.<sup>22</sup> On

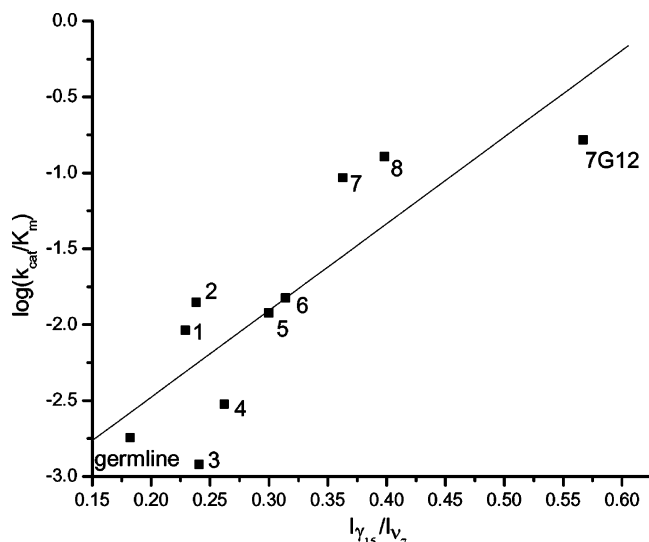


**Figure 9.** Correlation of catalytic efficiency ( $\log(k_{cat}/K_m)$  from ref 2) with  $\gamma_{15}$  activation (intensity relative to the adjacent  $\nu_7$  band) for MP bound to the 7G12 antibody variants in this study.

the basis of these collective studies, it has been proposed<sup>1</sup> that the intrinsic structural plasticity like sequence diversity contributes to the tremendous binding potential of the germline antibody repertoire. Somatic mutations then fix the combining site conformation of the affinity-matured antibody to bind a specific ligand with high affinity in a locked key fashion. Furthermore, it was argued that in the case of antibody 7G12 the increase in rigidity and binding affinity during affinity maturation leads to increased distortion of the mesoporphyrin substrate and, as a consequence, an increased catalytic rate.<sup>2</sup>

In this study the RR spectra of the Fab-bound MP were used to follow the extent of substrate distortion and thus the extent of strain applied to the MP substrate by the antibody combining site. The distortion of MP in the germline Fab, the 7G12 Fab, and various mutants with different somatic mutations are compared on the basis of the  $I(\gamma_{15})/I(\nu_7)$  ratio, which increases with a higher extent of out-of-plane porphyrin distortion. This analysis clearly shows that the affinity-matured antibody distorts that substrate more than the germline antibody, which is consistent with the enhanced binding energy and catalytic efficiency of 7G12.

As shown in Figure 5, the somatic mutations Ser97<sup>H</sup>Met, Arg50<sup>H</sup>Met, and Ala32<sup>H</sup>Pro all increase porphyrin distortion significantly. When residues at these positions are each switched back individually to their germline identities, the  $I(\gamma_{15})/I(\nu_7)$  ratio of Fab-bound MP drops 40–50% compared to that of the affinity-matured 7G12 Fab. Likewise, they display intermediate catalytic efficiencies as measured<sup>2</sup> by  $k_{cat}/K_m$ . Figure 9 shows a reasonable correlation between the logarithm of this ratio and the  $\gamma_{15}/\nu_7$  intensity. The roughly linear dependence indicates that the  $\gamma_{15}$  activation is largely proportional to the activation energy, as expected if the distortion stabilizes the transition state. The structural studies revealed that somatic mutations Arg50<sup>H</sup>Met and Ser97<sup>H</sup>Met fix the conformation of the CDRH3 loop for binding a distorted MP, and Ala32<sup>H</sup>Pro reinforces the packing of Tyr91<sup>L</sup> (CDRL3) on pyrrole ring A of the bound MP. In addition, comparison of  $I(\gamma_{15})/I(\nu_7)$  for mutants 1–3 with that of mutants 5–7 suggests that, as more somatic mutations accumulate, the antibody applies more strain to the

(19) Yin, J.; Beuscher, A. E.; Andryski, S. E.; Stevens, R. C.; Schultz, P. G. *J. Mol. Biol.* **2003**, *330*, 651–656.

(20) Wedemayer, G. J.; Patten, P. A.; Wang, L. H.; Schultz, P. G.; Stevens, R. C. *Science* **1997**, *276*, 1665.

(21) Mundorff, E. C.; Hanson, M. A.; Varvak, A.; Ulrich, H.; Schultz, P. G.; Stevens, R. C. *Biochemistry* **2000**, *40*, 627.

(22) Yin, J.; Mundorff, E. C.; Yang, P. L.; Wendt, K. U.; Hanway, D.; Stevens, R. C.; Schultz, P. G. *Biochemistry* **2001**, *40*, 10764.

MP substrate and the antibody combining site becomes more rigid. Thus, during affinity maturation, somatic mutations are selected that increase the binding affinity of antibody 7G12 with NMP and at the same time preorganize the antibody combining site to stabilize the nonplanar conformation of the porphyrin molecule for metalation. In summary, the affinity maturation of antibody 7G12 recapitulates the evolution of enzymatic

function in which the binding energy is evolved to lower the activation energy of a reaction, in this case by straining the substrate.

**Acknowledgment.** The work was supported by NIH Grant GM 33576 (to T.G.S.) and NIH Grant GM 56528 (to P.G.S.).

JA0465395